ELSEVIER

Atmospheric Research 47–48 (1998) 41–58

ATMOSPHERIC RESEARCH

Linear eddy modeling of droplet spectral evolution during entrainment and mixing in cumulus clouds

Chwen-Wei Su [a], Steven K. Krueger [b,*], Patrick A. McMurtry [a], Philip H. Austin [c]

[a] *Department of Mechanical Engineering, University of Utah, Salt Lake City, UT 84112, USA*
[b] *Department of Meteorology, University of Utah, Salt Lake City, UT 84112, USA*
[c] *Atmospheric Sciences Programme, University of British Columbia, Vancouver, BC, Canada V6T1Z2*

Accepted 7 May 1997

Abstract

The explicit mixing parcel model (EMPM) of Krueger et al. [Krueger, S.K., Su, C.-W., McMurtry, P.A., 1997. Modeling entrainment and fine-scale mixing in cumulus clouds. J. Atmos. Sci. 54, 2697–2712.] is extended to explicitly account for individual droplet growth. The model provides a 1D representation of physical properties within a cloud parcel and incorporates the rising of the cloud parcel, entrainment of environmental air into the parcel, finite-rate turbulent mixing parameterized by Kolmogorov inertial range scalings, and droplet growth. Because the simulation is performed in a 1D domain, all relevant length scales of the mixing process can be resolved. For the typical domain size used (20 m) in this study, the growth of approximately 2000 droplets is explicitly calculated based on their local environments. Comparisons of computed droplet spectra with spectra obtained from airplane penetration exhibit good agreement. Further results showing effects of entrained CCN, droplet sedimentation and mixing rates on droplet spectral evolution are provided.

Keywords: Linear eddy modeling; Turbulent mixing; Droplet growth; Cumulus clouds

1. Introduction

Reliable predictions of cloud droplet size distributions can lead to better understandings of many important atmospheric problems including warm rain initiation, cloud

* Corresponding author. Fax: +1-801-585-3681; e-mail: skrueger@atmos.met.utah.edu

0169-8095/98/$19.00
PII S0169-8095(98)00039-8

chemical reactions, cloud radiative properties, and cloud dynamic processes. Classic adiabatic parcel models generally predict narrow and single peaked droplet spectra. On the other hand, data gathered from in-cloud measurements in cumulus clouds usually exhibit bimodal and broad droplet spectral shapes. Although much effort has been directed at developing models to realistically simulate droplet spectral evolution in cumulus clouds, the problem remains unresolved.

Several ideas have been put forward to explain the broadening of the droplet spectrum and large droplet formation in cumulus clouds. For example, the presence of giant aerosols have been suggested as the causes of larger droplet formation (Johnson, 1982). Srivastava (1989) showed that droplet spectral widths can be broadened by using the local microscopic supersaturation environment without considering effects of turbulence on the droplet. Also, mixing of parcels with different trajectories may possibly lead to significantly broad droplet spectra (Telford and Chai, 1980; Cooper, 1989).

The effects of entrainment and mixing on droplet spectra also constitute an active area of research. The first studies in this area assumed continuous entrainment of dry air into cloud and subsequent instantaneous mixing (e.g., Warner, 1973; Mason and Jonas, 1974; Lee and Pruppacher, 1977).

Baker and Latham (1979) and Baker et al. (1980) argued that the finite rate of mixing is an important factor in the evolution of the cloud. These works involved dimensional analysis to show that the droplet evaporation time scale is usually much smaller than the mixing time scale. In their model, the mixing of environmental dry air into cloudy air will completely evaporate some droplets in regions adjacent to dry clear air until the entrained blob becomes saturated. This mixing mechanism can be referred to as extremely inhomogeneous mixing.

The Broadwell and Breidenthal (1982) picture of shear layer entrainment and mixing provides a useful framework to conceptualize the physical turbulent mixing process. During turbulent mixing, entrained parcels of fluid are stretched out and intertwined during the eddy break-down process. The actual mixing of the entrained fluid is a molecular diffusion process that is most effective after scalar length scales have been reduced to diffusion length scales (on the order of the Kolmogorov scale for gases). This turbulent mixing picture is consistent with in-cloud observations that show abrupt transitions between uniform regions and adjacent regions containing large variability. Recent observational analyses provide strong evidence that such a mixing mechanism exists in cloud (e.g., Baker, 1992; Brenguier, 1993). The observational studies suggest the following conceptual picture of mixing: a cloud engulfs discrete blobs of clear air. Subsequent to this entrainment, deformation and stretching occur, reducing scalar length scales at a finite rate. As the length scales decrease, molecular mixing increases as a result of increased scalar gradients. Under such a mixing process, the droplet growth (or evaporation) processes are dependent on their local microphysical environments.

Rigorously modeling entrainment and mixing processes in cumulus clouds using a finite-rate mixing approach is a challenge because of the large range of length scales that exist. For a typical cumulus cloud, the largest length scale is on the order of 1 km, while the smallest eddy size is on the order of 1 mm. Limitations in computational resources demand that for multi-dimensional calculations, small-scale processes be parameterized (e.g., Brenguier and Grabowski, 1993).

An alternative to multi-dimensional simulations is to employ 1D models with parameterized turbulent mixing. Jensen and Baker (1989) used a simplified mixing model to study droplet spectral evolution in a parcel after one entrainment event. The mixing process in their model was represented by a single eddy which was compressed as time elapsed. Grabowski (1993) used a similar approach by specifying a fixed strain rate for the mixing process. A shortcoming associated with above models is that only one length scale (eddy size) participates in the mixing process.

A novel 1D formulation of turbulent mixing has been recently developed and extensively applied to a variety of turbulent mixing processes. The model, termed the linear eddy model (LEM), was developed by Kerstein (1988) and explicitly treats the two primary mechanisms of turbulent mixing: (1) the reduction in length scale by turbulent deformation from a spectrum of turbulent length scales, and (2) molecular diffusion. Turbulent deformation is treated in a stochastic manner and accounts for the effects of eddy size distribution, while molecular diffusion is treated deterministically by solution of the 1D diffusion equation.

Recently, the LEM has been incorporated with bulk microphysics to study entrainment and mixing in cumulus clouds (Krueger et al., 1997, hereafter KSM). In this work, the linear eddy model of turbulent mixing was combined with a parameterization of entrainment to predict the evolution of thermodynamic quantities in a rising cumulus cloud parcel. This explicit mixing parcel model (EMPM) was applied to study the entrainment and mixing for Hawaiian trade cumulus clouds. The model results agreed well with observed in-cloud means and variances.

For the present study, the EMPM has been extended to include explicit microphysical calculations. Of particular focus is the prediction of the droplet spectral evolution during entrainment and mixing in cumulus clouds. In this paper, we present results from a number of simulations using this approach. Comparisons are provided with droplet spectra obtained from Hawaiian cumulus cloud measurements. The model parameters are then varied to study the effects of entrainment, mixing rate, entrained CCN properties, and droplet sedimentation on droplet spectral evolution.

2. Model description

The EMPM has been described in detail in KSM so only a general overview is provided here. The following generalized picture of entrainment and mixing in cumulus clouds is adopted in the EMPM: Initially, a parcel of cloudy air containing cloud droplets rises from cloud base. As the parcel rises, it intermittently entrains blobs of environmental air. Meanwhile, turbulent deformation and molecular diffusion are ongoing processes within the cloud. Droplets within the cloud grow or evaporate depending on their local microphysical environments.

The EMPM provides a 1D spatial description of the evolution of a rising cloud parcel subject to the above picture. The 1D formulation is necessary to obtain the high degree of spatial resolution required to accurately predict droplet formation in a turbulent environment. The key to obtaining reliable simulations is to provide a realistic treatment of turbulent mixing within the 1D description.

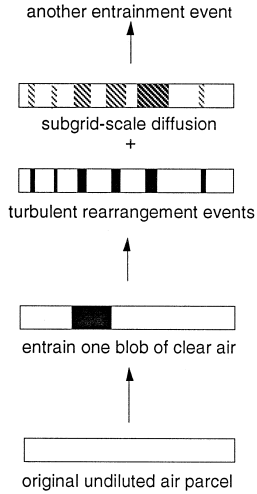

Fig. 1. Schematic diagram of EMPM's implementation on the entrainment and mixing processes in cumulus clouds: a parcel of undiluted cloudy air entrains environmental dry clear air. The mixing process is represented by the linear eddy model. First, the mixed parcel is stretching because of the large turbulent motions, then the molecular diffusion smooths out the sharp interfaces.

Fig. 1 is a schematic representation of the main processes represented in the EMPM. Four processes are considered in the model: parcel ascent, entrainment, turbulent mixing (i.e., turbulent deformation and molecular diffusion), and droplet growth. The parcel's ascent rate is specified. Entrainment occurs in discrete events. During each event, a randomly selected region of the parcel is replaced with environmental air. The size of the entrained blob is a specified parameter and the mean frequency of entrainment is chosen to be consistent with the observed fractional rate of entrainment. Turbulent mixing and droplet growth (or evaporation) processes are explicitly treated by the LEM and by solution of the droplet growth equation, respectively. The implementation of these processes is briefly described below.

2.1. Entrainment in the EMPM

To include discrete entrainment events, the fractional entrainment rate, λ, and the size of the entrained blobs must be specified. The fractional entrainment rate, defined as $\lambda = \frac{1}{m}\frac{\mathrm{d}m}{\mathrm{d}z}$, where m is the parcel mass, z is height, is estimated from observational data (see Section 3).

Selection of the entrained blob size is more difficult to rigorously pin down. In cumulus clouds, entrained blobs have a range of sizes. Because of our lack of knowledge about this process, we simply specify a constant blob size d. For computational efficiency, the domain size remains fixed throughout a simulation, therefore, an entrainment event replaces a segment of the parcel's cloudy air with entrained air. The location of the entrained blob is randomly chosen. The removal of randomly selected segments does not affect the parcel's statistical properties because the model is designed to be statistically homogeneous.

The average height interval, $(\Delta z)_{\text{avg}}$, between entrainment events is:

$$(\Delta z)_{\text{avg}} = \frac{1}{\lambda}\frac{d}{D-d} \tag{1}$$

where D is the domain size. The actual interval Δz, for each entrainment event is selected from an exponential distribution with mean $(\Delta z)_{\text{avg}}$.

The remaining unknown in Eq. (1) is the entrained blob size. We assume that it is related to the chosen domain size, D. The ratio $\sigma \approx d/D$ is the fraction of the domain occupied by entraining air during an entrainment event. In a thermal, we can interpret σ as the fractional area of the thermal's surface occupied by entraining air. Then $\sigma = w_e/w_*$, where w_e is the average entrainment velocity, and w_* is the characteristic velocity of the entraining eddies. We assume that $w_* \sim w$, where w is the parcel rising velocity, and that $w_e = \alpha w$. Then $\sigma \sim \alpha$. Laboratory experiments suggest that $\alpha \sim 0.2$ for a spherical parcel (Cotton, 1975). However, conventional entraining parcel model studies indicate that values of α about half as large are needed to accurately predict cumulus cloud top height (Cotton, 1975). Therefore, we set $\sigma = 0.1$.

In KSM, the domain size was chosen to be close to the cloud's width. A range of 500 to 2000 m for D was used. The corresponding range for $d = \sigma D$ is then 50 to 200 m.

Signatures of entrainment events appear to exist in cumulus clouds. Raga et al. (1990) identified relatively homogeneous regions as such signatures. They found that the average width of such regions, which they called the 'entrainment length', was a few hundred meters for the Hawaiian trade cumuli they studied. Such regions would be larger than the associated entrained blob size. The observed entrainment lengths are therefore in accord with our estimated range of entrained blob sizes.

In the present study, we cannot afford to perform simulations with large domain sizes due to the complicated droplet growth calculations and the need to more finely resolve the small scales. In most of our simulations, the domain size is 20 m. The entrained blob size is then 2 m using the same ratio $\sigma = 0.1$. A simulation with a larger domain size of 100 m was performed to test the sensitivity to domain size; in that case, the entrained blob size was 10 m. The 100-m results are similar to those from the 20-m case. The reason for insensitivity of the results to the initial entrained blob size is that droplet growth or evaporation is an inherently small-scale process and is not affected by entrainment until scalar length scales have been reduced to near the diffusion scales. As a result a 100-m parcel with a 10-m entrained blob involves a cascade process that must break down the entrained blob to smaller scales before droplet growth or evaporation is significantly affected. A 10-m blob thus takes longer to mix, but eventually produces the same effects at the small scales as a 2-m blob.

2.2. The linear eddy model

The EMPM utilizes the linear eddy model to simulate high-Reynolds number mixing in one spatial dimension. The model, which has been extensively used in a wide range of mixing studies (e.g., Kerstein, 1991), retains a distinction, at all scales of the flow, between the two key features in turbulent mixing: molecular diffusion and turbulent deformation. Molecular diffusion is accomplished by the numerical solution of the

diffusion equation, $\partial c/\partial t = D_M(\partial^2 c/\partial x^2)$ over a linear domain in which the scalar field is highly resolved. This diffusion process is punctuated by random rearrangements of the scalar field, representing the turbulent advection process. Rearrangements occur at a frequency based on the specified turbulence diffusivity, D_T. The rearrangement event size is randomly chosen from an eddy distribution based on the Kolmogorov cascade picture of high-Reynolds number turbulence (Kerstein, 1991).

Each rearrangement event is described by the 'triplet map', which involves a three-fold compression of the scalar field in the selected interval of the spatial domain. The triplet map replaces the scalar field within the interval by three copies of the compressed image, and inverts the central image. This formulation captures the effects of the stretching and folding mechanisms responsible for mixing in turbulent flow.

Rearrangement event sizes range from η to L, which are the model Kolmogorov and model integral scales. The input parameters thus required in the linear eddy model are the molecular and turbulent diffusivities, D_M and D_T; the model integral scale, L, and the model Kolmogorov scale, η. For relating model parameters to cloud processes, we use the relation $D_T L^{4/3}\epsilon^{1/3}$, where ϵ is the dissipation rate.

2.3. The droplet growth equations

In the model presented here, the growth of each individual droplet is calculated. Each droplet's diffusional growth is explicitly calculated based on its local environmental conditions. The droplet's diffusional growth is described by (Fukuta and Walter, 1970):

$$r_j \frac{\mathrm{d}r_j}{\mathrm{d}t} = \frac{S - A_1 + A_2}{A_3 + A_4}, \tag{2}$$

where r_j is the radius of the jth droplet; A_1 and A_2 are the correction factors for droplet curvature and solution effects; A_3 and A_4 are the heat conduction and the vapor diffusion terms (see Appendix A for terms A_1 to A_4). S is the supersaturation ratio:

$$S = \frac{q_v}{q_{vs}} - 1, \tag{3}$$

where q_v is the water vapor mixing ratio and q_{vs} is the saturated water vapor mixing ratio.

The droplets grow (or evaporate) depending on their local environment. Of particular importance to the droplet growth process are temperature (T) and water vapor (q_v). These are both affected by molecular diffusion and phase changes. The governing equations for changes due to phase changes are:

$$\frac{\mathrm{d}q_v}{\mathrm{d}t}\Big|_{\text{phase change}} = -\sum_j 4\pi N_j \rho_w r_j^2 \frac{\mathrm{d}r_j}{\mathrm{d}t}, \tag{4}$$

and:

$$\frac{\mathrm{d}T}{\mathrm{d}t}\Big|_{\text{phase change}} = -\frac{L_v}{c}\frac{\mathrm{d}q_v}{\mathrm{d}t}\Big|_{\text{phase change}} - w\frac{g}{c}, \tag{5}$$

where N_j is the jth droplet concentration in the grid volume, ρ_w is the liquid water

density, L_v is the latent heat, and c is the heat capacity of the system of air, vapor and liquid water at constant pressure, w is the rising velocity, and g is gravity.

The values of q_v and T are also affected by molecular diffusion. The changes due to molecular diffusion are:

$$\frac{\partial T}{\partial t}\Big|_{\text{molecular diffusion}} = D_{\text{Temp}} \frac{\partial^2 T}{\partial x^2} \tag{6}$$

and:

$$\frac{\partial T}{\partial t}\Big|_{\text{molecular diffusion}} = D_v \frac{\partial^2 q_v}{\partial x^2}. \tag{7}$$

Here D_v is the water vapor diffusivity in air, and D_{Temp} is the thermal diffusivity of air.

The temperature decreases due to adiabatic expansion as the parcel rises. The change of the parcel's pressure is calculated using the hydrostatic equation.

In our simulation, Eqs. (2), (4) and (5) are solved using a fifth-order Runge–Kutta formula with an adaptive time step (Press et al., 1992).

3. Simulation parameters

3.1. Cloud base and environmental conditions

The input parameters for this study are taken from Hawaiian trade cumulus cloud measurements (Raga et al., 1990). The cloud base for these clouds ranged from 930 to 965 mb (430–750 m), the base of the trade inversion was at about 765 to 835 mb (1700–2450 m), and the cloud tops were generally a few hundred meters above the base of the trade inversion. The environmental profile has about 80% relative humidity below the trade inversion and about 20% above. In the present study, the cloud base conditions are taken to be $P_b = 963.95$ mb (450 m), $T_b = 293.95$ K and $q_v = 15.73$ g kg^{-1}.

The droplet spectrum is initialized as follows: a population of CCN is assumed to contain CCN at their equilibrium sizes at cloud base. These CCN are composed of 31 categories of ammonia bi-sulfate and 18 categories of salt. The CCN distribution is obtained using the normal mass distribution with respect to log diameter. The total concentration of CCN is about 100 cm^{-3}. This distribution is sampled and assigned to the model domain, 20 m $\times$ 1 mm $\times$ 1 mm. About 2000 droplets are obtained and assigned random locations within the domain. Each droplet subsequently grows (or evaporates) depending on its local environment as affected by parcel ascent, entrainment, mixing, and the growth of other droplets.

3.2. Entrainment and mixing parameters

The entrained blob size is obtained using the relation $d = \sigma D$ (see Section 2.1). In the present study, the domain size is 20 m, so the entrained blob size is 2 m. The fractional entrainment rate is 1.0 km^{-1} as estimated from Raga et al. The entrained blob contains a CCN distribution which is taken to be the same as at cloud base. These CCN

are assigned their equilibrium sizes which depend on the relative humidity at the entrainment height. The CCN can be entrained into the cloudy parcel and then participate in the droplet growth process.

The mixing parameters are L, η, D_T and D_M. For the Hawaiian trade cumuli, Raga et al. reported that the active cloud turrets were 2 to 3 km wide. This sets an upper bound on L since it cannot be larger than the observed cloud width. Cumulus clouds consist of many thermals with internal circulations, so L may be significantly less than the cloud width. In our earlier paper (KSM) we set $L = 500$ m. In our current simulation, the domain size D is 20 m. The largest possible eddy size, L, is set equal to the domain size, D. In other words, we did not simulate the larger eddies (greater than 20 m). This will not be matter much. because the larger eddy sizes (from 20 m to 500 m) are relatively infrequent and will not have significant effects on the turbulent mixing processes.

We can use L and the measurement of the turbulent kinetic energy dissipation rate ϵ to specify D_T. The result is $D_T \approx 0.1\ L^{4/3}\epsilon^{1/3}$ (Krueger, 1993), where L is the largest eddy size used in the EMPM. We use $\epsilon = 0.01\ \mathrm{m^2\ s^{-3}}$ in the baseline case.

The physical Kolmogorov scale is 1.2 mm for a cumulus cloud with $\epsilon = 0.01\ \mathrm{m^2\ s^{-3}}$. In the present studies, the model Kolmogorov scale (the smallest eddy size used in the simulation), η is 10 mm. When the physical Kolmogorov scale is not resolved, the effects of eddies smaller than the model's smallest eddy size, η, are simply parameterized by the subgrid-scale diffusivity. The molecular diffusivity is replaced by the turbulent diffusivity due to eddies smaller than η. This is $D_T(\eta/L)^{4/3}$ (Tennekes and Lumley, 1972). The results from a sensitivity test showed that the droplet spectra were very similar for the cases with $\eta = 10$ mm and $\eta = 1.2$ mm.

Table 1
Nominal input parameters for simulations

Parameter	Value
Cloud base conditions	
P_b	963.95 mb
z_b	450 m
T_b	293.95 K
q_v	15.73 g $\mathrm{kg^{-1}}$
n	100 $\mathrm{cm^{-3}}$
Entrainment parameters	
λ	1.0 $\mathrm{km^{-1}}$
w	2.0 m $\mathrm{s^{-1}}$
$\sigma = d/D$	0.1
D	20 m
d	2 m
Mixing parameters	
ϵ	0.01 $\mathrm{m^2\ s^{-3}}$
L	20 m
η	0.01 m
$\Delta x = \eta/6$	1.67 mm

The grid size Δx is chosen so that η is the size of the smallest segment that undergoes rearrangement events. When using the triplet map, six grid cells are the minimum that can participate in a rearrangement event. Therefore, $\Delta x = \eta/6 \approx 1.67$ mm.

Table 1 summarize the above parameters. It should be noted that the above parameters are the nominal values used in our simulations. Results are presented in the following in which these parameters are individually varied to isolate and understand their effects on droplet spectral evolution. The parameters varied include entrained CCN, the turbulent dissipation rate, and droplet sedimentation. Because we found that droplet sedimentation does not result in much difference in droplet spectra for the nominal value of dissipation rate used (see Section 4.4), unless otherwise noted, droplet sedimentation is not included. Unless otherwise stated, entrained air contains CCN.

4. Simulation results

4.1. Comparisons with measurements

We first compare our simulation results with aircraft measurements from a Hawaiian trade cumulus cloud. These measurement were taken during the Joint Hawaii Warm Rain Project during the summer of 1985. For details of this experiment and data analysis, see Raga et al. (1990) and Hicks et al. (1990). The specific cloud for our comparisons was designated as cloud 9, 10 July 1985 (Pontikis and Hicks, 1993). The cloud droplet spectra were measured by the Forward-Scattering Spectrometer Probe (FSSP) with a sampling frequency of 10 Hz ($\sim$ 10 m). Six penetrations were made at 960 mb, 907 mb, 860 mb, 810 mb, 760 mb and 720 mb. The cloud base conditions, P_b, T_b and q_v were very close to the composite values listed in Table 1. Our EMPM results were obtained using the parameters listed in Table 1 except that the droplet concentration at cloud base was changed to 205 cm^{-3} to better match the corresponding measurement. The comparisons are presented for three levels below the trade inversion, 907 mb, 860 mb and 810 mb. In the field measurements, many droplet samples were obtained during each penetration. Although the droplet spectral shapes were different for each 10 m sampled size, the general trend was similar. We have chosen two representative sections for our comparison at each level.

The measured and predicted droplet spectra are shown in Fig. 2. The EMPM results appear to agree quite well in terms of the droplet spectral width and exhibit the same trend of spectral evolution at different heights. Quantitative differences in the largest droplet size, overall concentration, and appearance of a single peak are, however apparent. The reasons behind these differences are not immediately evident. Quantitative differences can be expected due to the parameterization of entrainment. Furthermore, uncertainty in the specification of model parameters is also a concern. For example, the initial droplet distributions and entrained CCN properties, the size of the entrained blob, and the parcel rising velocity, all affect the droplet spectra and may vary within a cloud. Despite the quantitative differences, the comparisons shown in Fig. 2 provide confidence that the EMPM model results can be used as a tool to perform the parametric studies to

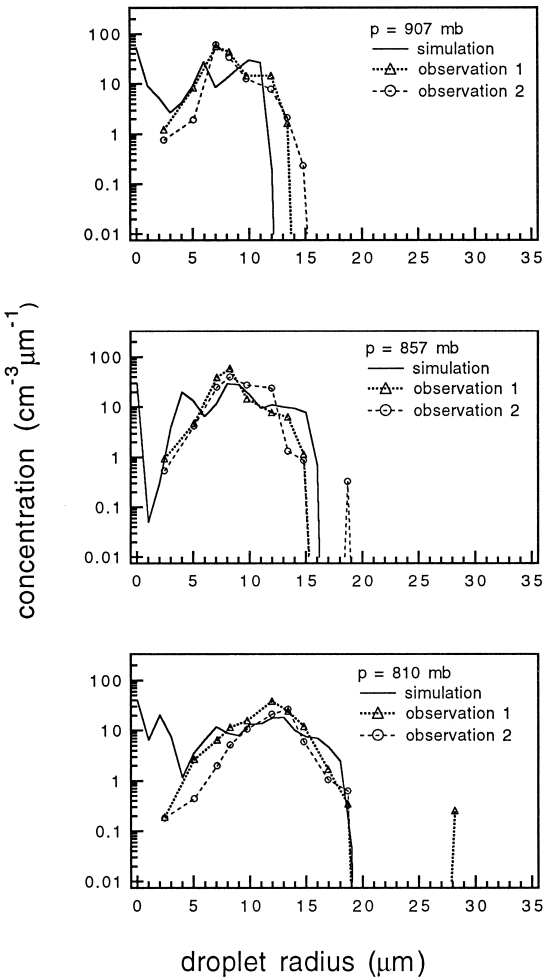

Fig. 2. Comparisons of EMPM results with observed droplet spectra from a Hawaiian trade cumulus cloud at three different levels. The plain solid line represents the results from a simulation. The two marker lines are two observational sections of 10-m size during the same aircraft penetration.

isolate the effects of specific parameters. It also should be noted that the comparisons between the finite-rate mixing case and observation are much better than the simulated results obtained from an adiabatic parcel model or an instant mixing model with multiple entrainment events (see Fig. 3 in Section 4.2).

4.2. General effects of entrainment and mixing on cloud droplet spectra

Fig. 3 shows the droplet spectral evolution for three different cases: adiabatic ascent (no entrainment), instant mixing (with discrete entrainment events), and finite-rate mixing (also with discrete entrainment events). Each frame in a column shows the

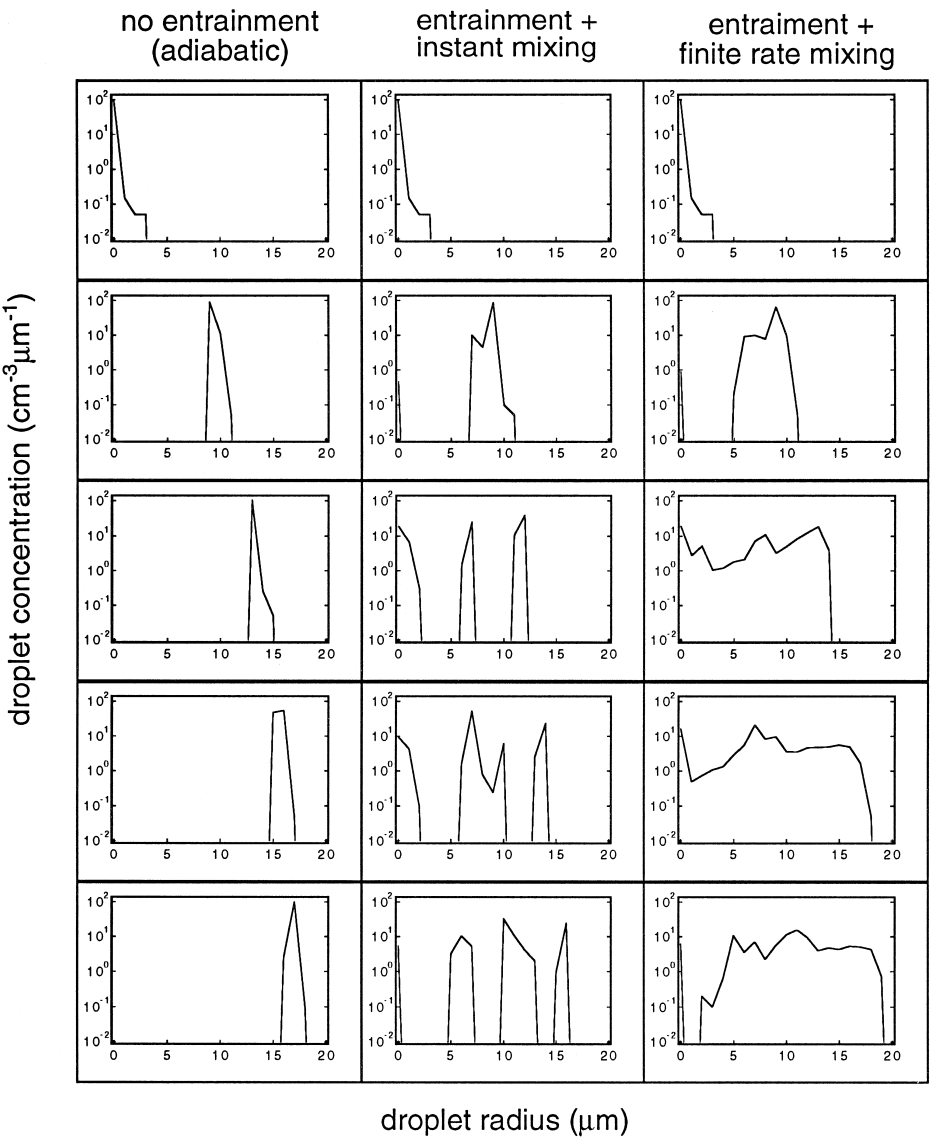

Fig. 3. Droplet spectra at different heights from cloud base to 1100 m. The left, middle and right columns are adiabatic, instantaneous mixing and finite-rate mixing cases, respectively.

droplet spectrum at a different height, from cloud base (top frame) to 1.1 km above cloud base (bottom frame). For the instant mixing and finite-rate mixing cases, the input parameters are the same as Table 1.

The adiabatic case exhibits a narrow droplet spectrum that simply shifts to larger droplet sizes as the parcel rises. The predominant feature of the instant mixing is the

development of multiple isolated peaks. Upon entrainment of dry air, evaporation can occur, but as the parcel rises, small droplet growth is rapid as a result of the instant mixing of entrained CCN that are activated after entrainment. Because the pre-existing droplets are much larger than the newly-activated ones, the development of isolated peaks results. For finite-rate mixing (third column), a broad droplet spectrum develops. This occurs because the finite mixing rate leads to significant fine-scale structure which allows individual droplets to experience quite different local environments, resulting in different growth rates. The comparisons for the three cases shown here indicate better agreement between the simulated finite-rate mixing case and observations (see Section 4.1, Fig. 2) than with an adiabatic parcel model or with an instant mixing model with entrainment.

It is noteworthy that the finite-rate mixing case has a largest droplet size of 19 μm at 1.1 km above cloud base compared with 18 μm for the adiabatic case and 16 μm for the instant mixing case. The total droplet concentration in the finite-rate mixing case is almost the same as in the adiabatic case at 1.1 km above cloud base. The results indicate superadiabatic droplet growth in the finite-rate mixing case.

4.3. The effects of entrained CCN

Fig. 4 shows the effects on the droplet spectral evolution of including CCN in the entrained air. To isolate the effects of the entrained CCN from other effects, only one entrainment event is allowed (at 250 m above cloud base). The domain size is 20 m. The size of the entrained blob is 6 m. Results are shown for a case with entrained CCN and one without, with all other parameters identical. Fig. 4a shows the spectrum prior to entrainment. After the entrainment event, the spectra begin to broaden due to partial

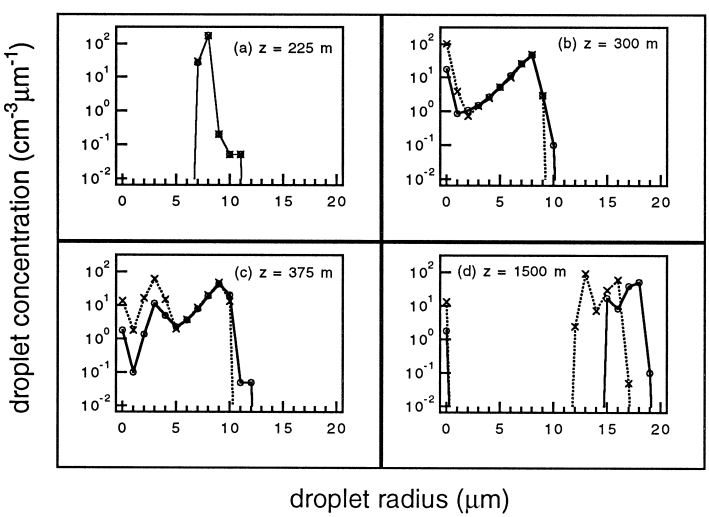

Fig. 4. Simulated droplet spectra at different heights. One entrainment event occurs at 250 m above cloud base. Dotted line: CCN entrained. Solid line: no CCN entrained.

evaporation of some droplets while other droplets totally evaporate (Fig. 4b). As the parcels continue to rise, CCN are activated and grow into small droplets (see the peaks of small droplet radius in Fig. 4c). Finally, in Fig. 4d, we note that with entrained CCN, the droplet sizes are generally smaller than without entrained CCN. This is a result of more droplets in the entrained CCN case competing for the same amount of water vapor.

4.4. The effects of sedimentation

The effects of sedimentation on droplet spectral evolution are generally thought to result in broadened spectra. When a parcel entrains a blob of clear air, gravity can cause droplets to fall into the subsaturated air, thus modifying the droplet spectrum. Baker et al. (1984) used a simple scale analysis to show that droplet sedimentation may eliminate the water vapor deficit in the undersaturated entrained air before the mixing is completed. Paluch and Knight (1984) used a simple model of droplet sedimentation and evaporation at the boundaries between unsaturated air and cloud air to illustrate the potential broadening effects of sedimentation on droplet spectra. Jensen and Baker (1989) similarly showed that sedimentation can have a broadening effect on droplet spectra. Although these works have illustrated mechanisms by which sedimentation

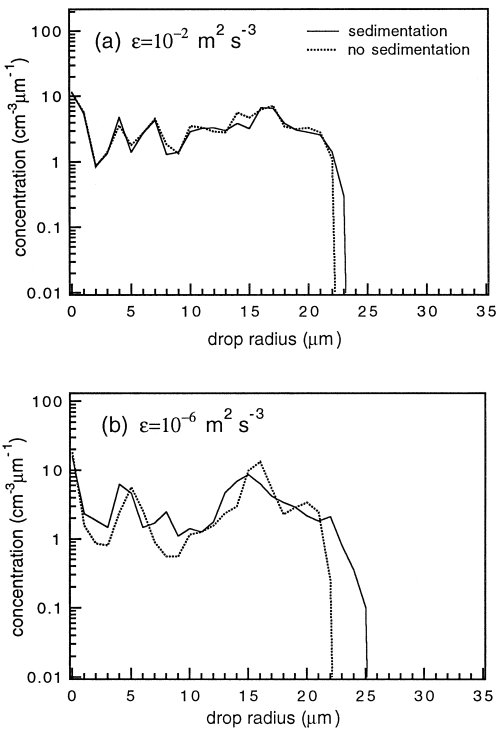

Fig. 5. Comparisons of droplet spectra at 1500 m above cloud base for the cases with and without droplet sedimentation. (a) A fast-mixing case with turbulent dissipation rate $\epsilon = 10^{-2}$ m^2 s^{-3}. (b) A slow-mixing case, $\epsilon = 10^{-6}$ m^2 s^{-3}.

affects the droplet spectral evolution, the quantitative effect of sedimentation under more realistic conditions has not been adequately explored.

To study this effect in the EMPM, each droplet's terminal velocity is calculated based on Stoke's law. The droplets fall through the assumed vertically-oriented domain with this terminal velocity. The periodic boundary condition was used, so as a droplet exited the domain, it was reinjected at the other boundary. Fig. 5 shows the simulated results at 1500 m above cloud base for two different turbulent dissipation rates, $\epsilon = 10^{-2}$ and 10^{-6} m^2 s^{-3}. We first see for fast mixing ($\epsilon = 10^{-2}$) that the droplet spectra are quite similar for the two cases, although sedimentation results in a few larger droplets. For slow mixing, however, a significantly broadened spectrum develops when sedimentation is included (Fig. 5b). The general trend of these results is in agreement with the studies cited above. However, the differences are significant only at low mixing rates. At high mixing rates, the change in environment seen by the droplets due to sedimentation is a secondary effect compared to changes in environment due to turbulent mixing. At low mixing rates, the parcel environment is homogenized more slowly so more droplets experience subsaturated air before the mixing is completed.

4.5. The effects of variations in mixing rate

The effects of changing the mixing rate are considered in this section. We first compare the spectral evolution for three different turbulent dissipation rates, $\epsilon = 10^{-2}$, 10^{-4} and 10^{-6} m^2 s^{-3}. The physical Kolmogorov scale is resolved for these runs and is 1.2 mm, 3.6 mm, and 12 mm, respectively. The domain size was also changed to 5 m due to the longer computer time required to carry out the simulations. The entrained blob size is 0.5 m. The total droplet number in each simulation is 500. Fig. 6 shows the droplet spectra for these three cases at 1435 m above cloud base. The size and concentration of the largest droplet is generally a little larger for the slower mixing rates.

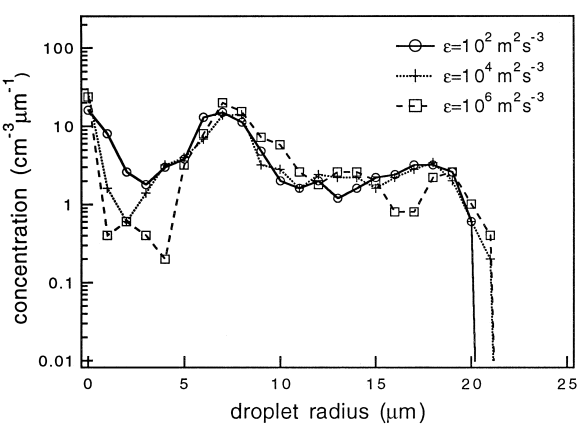

Fig. 6. Comparisons of droplet spectra at 1435 m above cloud base for three different turbulent dissipation rates, $\epsilon = 10^{-2}$, 10^{-4}, and 10^{-6} m^2 s^{-3}. The domain size for this simulation is 5 m. The entrained blob size is 0.5 m.

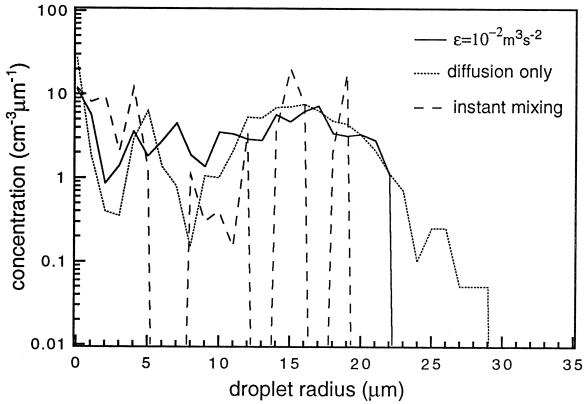

Fig. 7. Comparisons of droplet spectra at 1500 m above cloud base for instant mixing, finite-rate mixing ($\epsilon = 10^{-2}$ m^2 s^{-3}) and diffusion-only (no turbulent stirring) cases. The simulation domain size is 20 m, the entrain blob size for each entrainment event is 2 m.

We also compared the finite-rate mixing case with two extreme mixing scenarios, instantaneous mixing and diffusion-only (no turbulent stirring). The domain size for this study was 20 m with entrained blob size of 2 m. The total droplet number in these simulations here is 2000. The other input parameters are the same as listed in Table 1 for the comparison of diffusion-only, instant mixing, and finite-rate mixing cases. The simulated Kolmogorov scale is 10 mm. Fig. 7 shows the three different spectral shapes for these cases. We can see that the diffusion-only case develops the widest droplet spectrum while the instant mixing case has the narrowest one. The clear trend in Fig. 7 can be explained by the different environments the droplets experienced during the entrainment and mixing process. For the diffusion-only case, the inhomogeneity caused by random droplets locations and entrainment enables the individual droplets to experience very different environments which allows some to grow to very large sizes. The largest droplet in this case can grow to 29 μm at 1500 m above cloud base. For the instant mixing case, the droplets all experience the same uniform environment. For the finite-rate mixing case, turbulent stirrings allow the droplets to see the different environments between the two extreme cases.

5. Conclusions

The explicit mixing parcel model, developed by Krueger et al. (1997) has been extended to study the effects of entrainment and mixing on droplet spectral evolution in cumulus clouds. Four processes are considered in this model: the ascent of the parcel, entrainment of clear air, turbulent mixing (i.e., turbulent deformation and molecular diffusion), and individual droplet growth. The parcel's ascent rate is specified according to the mean observational value. Entrainment occurs in discrete events. The size of the entrained blob is a specified parameter and the mean frequency of entrainment is chosen to be consistent with the observed fractional rate of entrainment. Turbulent mixing and

droplet growth (or evaporation) processes are explicitly treated. Turbulent mixing is carried out using a 1D turbulent mixing model, the linear eddy model. Growth (or evaporation) of droplets is calculated by a droplet growth equation.

Model results compare well with data obtained from Hawaiian trade cumulus clouds. Based on these results, a series of parametric studies were performed to provide insight into the effects of different physical processes on the evolution of droplet spectra. These studies revealed broadened droplet spectra and larger droplet formation for the finite-rate mixing case compared to the instant mixing and adiabatic cases. The differences between these cases indicate the importance of accounting for fine-scale mixing to reproduce observed droplet spectrum.

It was further shown that entrainment of CCN increases the peak concentration of small droplets and decreases large droplet formation when compared to entrained parcels without CCN. This apparently results from more droplets competing for the same amount of water vapor.

Droplet sedimentation can result in a few droplets larger by 1 μm than without sedimentation when the mixing was fast. However, in a slower mixing case, sedimentation can broaden the droplet spectrum and result in droplets larger by 3 μm than without sedimentation.

Finally, we showed that different turbulent mixing rates characterized by a range of dissipation rates from 10^{-2} to 10^{-6} m^2 s^{-3} resulted in only small differences in the droplet spectral shapes. For the limiting cases of diffusion only and instant mixing, significant differences occurred. Namely, a broader spectrum for no stirring (diffusion only), and a narrower spectrum with isolated peaks for the instant mixing case, as previously mentioned.

Acknowledgements

The authors would like to thank Drs. C. Pontikis and G. Raga for kindly providing the measurement data. We also want to thank Dr. Jean-Louis Brenguier and an anonymous reviewer for their constructive comments. This work was supported in part by NSF Grant No. CTS9258445 and ONR grant N00014-91-J-1175. Our studies in mixing were also supported by the Advanced Combustion Engineering Research Center, the Utah Supercomputer Institute, and the Atmospheric Environment Service and National Science and Engineering Research Council of Canada. Funding for the Combustion Center is received from the National Science Foundation, the State of Utah, 26 Industrial participants, and the US Department of Energy.

Appendix A. Terms used in droplet growth equation

The terms of A_1 to A_4 in droplet growth equation, Eq. (2), are expressed as:

$$A_1 = \frac{2\hat{\sigma}}{R_v T \rho_l r_j} \tag{8}$$

$$A_2 = \frac{(i/M_s) M_w m_s}{(4/3)\pi r_j^3 \rho_l - m_s} \tag{9}$$

$$A_3 = \frac{\rho_l L_v^2}{f(\alpha) K_T R_v T^2} \tag{10}$$

$$A_4 = \frac{\rho_l R_v T}{f(\beta) D e_s} \tag{11}$$

where the symbols represent: $\hat{\sigma}$: droplet surface tension; R_v: gas constant for water vapor; T: temperature; ρ_l: liquid solution density; r_j: droplet radius at the jth class; i: the degree of ionic dissociation; m_s: mass of the solute; M_s: molecular weight of the solute; M_w: molecular weight of water; D: molecular diffusion coefficient of water vapor; e_s: saturation pressure over bulk water; L_v: latent heat; $f(\alpha)$: kinetic factor, $=[r/(r+l_\alpha)]$; $f(\beta)$: kinetic factor, $=[r/(r+l_\beta)]$; l_α: $K_T(2\pi M_d R_* T)^{1/2}/[\alpha P(c_v + R_*/2)]$; l_β: $(2\pi/R_v T)^{1/2}(D/\beta)$; α: thermal accommodation coefficient of air, use 1 in this simulation; β: condensation coefficient of water vapor, use 0.04 in this study; M_d: molecular weight of air; R_*: universal gas constant; c_v: specific heat at constant volume of air; K_T: thermal conductivity coefficient of air.

References

Baker, B., 1992. Turbulent entrainment and mixing in clouds: a new observational approach. J. Atmos. Sci. 49, 387–404.

Baker, M.B., Latham, J., 1979. The evolution of droplet spectra and the rate of production of embryonic raindrop in small cumulus clouds. J. Atmos. Sci. 36, 1612–1615.

Baker, M.B., Corbin, R.G., Latham, J., 1980. The influence of entrainment on the evolution of cloud droplet spectra: I. A model of inhomogeneous mixing. Q. J. R. Meteorol. Soc. 106, 581–598.

Baker, M.B., Breidenthal, R.E., Choularton, T.W., Latham, J., 1984. The effects of turbulent mixing in clouds. J. Atmos. Sci. 41, 299–304.

Brenguier, J.L., 1993. Observations of cloud microstructure at centimeter scale. J. Atmos. Sci. 32, 783–793.

Brenguier, J.L., Grabowski, W.W., 1993. Cumulus entrainment and cloud droplet spectra: a numerical model within a two-dimensional dynamical framework. J. Atmos. Sci. 50, 120–136.

Broadwell, J.E., Breidenthal, R.E., 1982. A simple model of mixing and chemical reaction in a turbulent shear layer. J. Fluid Mech. 125, 397–410.

Cooper, W.A., 1989. Effects of variable droplet growth histories on droplet size distributions: I. Theory. J. Atmos. Sci. 46, 1301–1311.

Cotton, W.R., 1975. Theoretical cumulus dynamics. Rev. Geophys. Space Phys. 13, 419–448.

Fukuta, N., Walter, L.A., 1970. Kinetics of hydrometeor growth from a vapor spherical model. J. Atmos. Sci. 27, 1160–1172.

Grabowski, W.W., 1993. Cumulus entrainment, fine-scale mixing, and buoyancy reversal. Q. J. R. Meteorol. Soc. 119, 935–956.

Hicks, E., Pontikis, C., Rigaud, A., 1990. Entrainment and mixing processes as related to droplet growth in warm midlatitude and tropical clouds. J. Atmos. Sci. 47, 1589–1618.

Jensen, J.B., Baker, M.B., 1989. A simple model of droplet spectral evolution during turbulent mixing. J. Atmos. Sci. 46, 2812–2829.

Johnson, D.B., 1982. The role of giant and ultragiant aerosols particles in warm rain initiation. J. Atmos. Sci. 39, 448–460.

Kerstein, A.R., 1988. Linear eddy modeling of turbulent scalar transport and mixing. Comb. Sci. Technol. 60, 391–421.

Kerstein, A.R., 1991. Linear eddy modeling of turbulent transport: Part 6. Microstructure of diffusive scalar mixing fields. J. Fluid Mech. 231, 361–394.

Krueger, S.K., 1993. Linear eddy modeling of entrainment and mixing in stratus clouds. J. Atmos. Sci. 60, 391–421.

Krueger, S.K., Su, C.-W., McMurtry, P.A., 1997. Modeling entrainment and fine-scale mixing in cumulus clouds. J. Atmos. Sci. 54, 2697–2712.

Lee, I.-Y., Pruppacher, H.R., 1977. A comparative study on the growth of cloud drops by condensation using an air parcel model with and without entrainment. Pure Appl. Geophys. 115, 523–545.

Mason, B.J., Jonas, P.R., 1974. The evolution of droplet spectra and large droplets by condensation in cumulus clouds. Q. J. R. Meteorol. Soc. 100, 23–38.

Paluch, I.R., Knight, C.A., 1984. Mixing and the evolution of cloud droplet size spectra in a vigorous continental cumulus. J. Atmos. Sci. 41, 1801–1815.

Pontikis, C.A., Hicks, E.M., 1993. Droplet activation as related to entrainment and mixing in warm tropical maritime clouds. J. Atmos. Sci. 50, 1888–1896.

Press, W.H., Flannery, B.P., Teukolsky, S.A., Vetterling, W.T., 1992. Numerical Recipes in FORTRAN: The Art of Scientific Computing. Cambridge Univ. Press, 963 pp.

Raga, G.B., Jensen, J.B., Baker, M.B., 1990. Characteristics of cumulus band clouds of the coast of Hawaii. J. Atmos. Sci. 47, 2708–2718.

Srivastava, R.C., 1989. Growth of cloud drops by condensation: a criticism of currently accepted theory and a new approach. J. Atmos. Sci. 46, 869–887.

Telford, J.W., Chai, S.K., 1980. A new aspect of condensation theory. Pure Appl. Geophys. 118, 720–742.

Tennekes, H., Lumley, J.L., 1972. A First Course in Turbulence, The MIT Press, 300 pp.

Warner, J., 1973. The microstructure of cumulus cloud: IV. The effect on the droplet spectrum of mixing between cloud and environment. J. Atmos. Sci. 30, 256–261.